Placenta and Reproductive Medicine

ORIGINAL ARTICLE

An effective and non-invasive prediction model for placenta accreta spectrum early diagnosis: Ultrasound image-based novel deep learning network

Wenyan Gao[1,#], Shuailin You[2,#], Yujiao Wu[2,#], Juan Su[2], Ziwei Li[1], Bei Shi[3,*], Xiran Jiang[2,*]

[1]Department of Obstetrics, the First Affiliated Hospital of China Medical University, Shenyang 110002, Liaoning Province, China
[2]School of Intelligent Medicine, China Medical University, Shenyang 110122, Liaoning Province, China
[3]Department of Physiology, School of Life Sciences, China Medical University, Shenyang 110122, Liaoning Province, China

ABSTRACT

Background: The study aimed to utilize ultrasound technology to capture quantitative features of placenta accuta spectrum (PAS) and assist in its early diagnosis.**Methods:** We proposed an EA-EffV2Net (an improved network combining EfficientNetV2 with an attention mechanism, where EA stands for Efficient Attention) model, trained and validated it by using ultrasound images from 468 pregnant women enrolled between July 2020 and January 2023. A clinical diagnostic model was developed based on important clinicopathological factors for comparison.**Results:** Our models can improve performance in both the detection of PAS and the differential diagnosis of placenta accreta (PA) and placenta increta (PI). Compared with the clinical diagnostic model, EA-EffV2Net generated slightly higher misdiagnosis rates when diagnosing PAS and PA.**Conclusions:** This study proposed a novel EA-EffV2Net model for the diagnosis of PAS and the differential diagnosis of PA and PI based on ultrasound images, which is suitable for all pregnant women is of clinical importance in individual treatment planning.

Keywords: placenta accreta, deep learning, ultrasonography, early diagnosis, obstetric labor complications

INTRODUCTION

Placenta accreta spectrum (PAS) has been known as a complex and high-risk obstetrical condition and is associated with significant maternal morbidity.[1,2] With cesarean section increased, the prevalence of PAS has increased significantly,[3–5] which increase the incidence of postpartum hemorrhage and infection.[6,7] PAS can be separated into three categories based on distinct pathological characteristics: placenta accreta (PA) refers to that villi attach directly to the myometrium surface without invasion; placenta increta (PI) refers to that villi penetrate deeply into the myometrium up to the external layer; placenta percreta (PP) means the villi invase through the full thickness of myometrium and even into organs adjacent to the uterus.[1,8] Villous adhesion or invasion is rarely evenly distributed in the myometrium, thereby limiting the accuracy of examination[10,12] and the clinical diagnosis of PAS can be made only by sampling through surgery or delivery.[9–12] A considerable number

[#]These authors contributed equally to this work.
***Corresponding Author:**
Xiran Jiang, M.D., Ph.D., School of Intelligent Medicine, China Medical University, Shenyang 110122, Liaoning Province, China. Email: xrjiang@cmu.edu.cn. https://orcid.org/0000-0002-9640-6368
Bei Shi, M.D., Ph.D., Department of Physiology, School of Life Sciences, China Medical University, Shenyang 110122, Liaoning Province, China. Email: bshi@cmu.edu.cn. https://orcid.org/0000-0001-8063-9100.
Received: 13 February 2026; Revised: 3 March 2026; Accepted: 14 March 2026
https://doi.org/10.54844/prm.2026.1183

of pregnant women who do not receive the indicationg of PAS existence experienced serious complications due to PAS during surgery or delivery. Therefore, a non-invasive and accurate methodology for PAS early diagnosis, which is suitable for all pregnant women is of clinical importance in individual treatment planning.

Ultrasound is the mainstay for PAS clinical imaging and non-invasive prenatal diagnosis,[13] which has improved in recent years.[14] However, numerous factors may affect diagnostic performance, including placental position and thickness, loss of hypoechoic space, and abnormalities of the uterus–bladder interface. Therefore, visual assessment of the ultrasound image and identification of PAS is both difficult and highly subjective. The application of quantitative image analysis techniques may be conducive to overcoming the subjectivity caused by visual inspections and improving diagnostic accuracy.

Deep convolutional neural networks (CNNs) is a promising technique in combination with the visual inspection method in the diagnosis and differential diagnosis of medical images,[15] which has been proven to work well for diagnosing various diseases,[16] but has not been studied for PAS. Here, we present a novel EA-EffV2Net model, which aims to assist clinicians identify PAS in all pregnant women from ultrasound images. Considering that PP can be diagnosised by existing ultrasound technology, our model is mainly studied for PA and PI.

METHODS

Study population

A total of 468 pregnant women, who were treated in the First Affiliated Hospital of China Medical University between July 2020 and January 2023, were enrolled, of which 216 had PAS and 252 did not. The study was approved by the ethics committee of the First Affiliated Hospital of China Medical University (No. 2024241). Participating women provided signed informed consent.

The inclusion criteria were patients who had (1) undergone an ultrasound examination one week before surgery or delivery, and (2) those with complete clinicopathological information. The exclusion criteria were patients with (1) a previous history of cesarean section, (2) abnormal placental position (low placenta or placenta previa), (3) a multiple pregnancy, (4) abnormal uterine anatomy, and (5) poor image quality. The inclusion/exclusion criteria of the patients are detailed in Figure 1. The clinicopathological data of the patients were collected from our hospital, and the privacy of all patients was protected by anonymizing both the ultrasound images and the clinicopathological data.

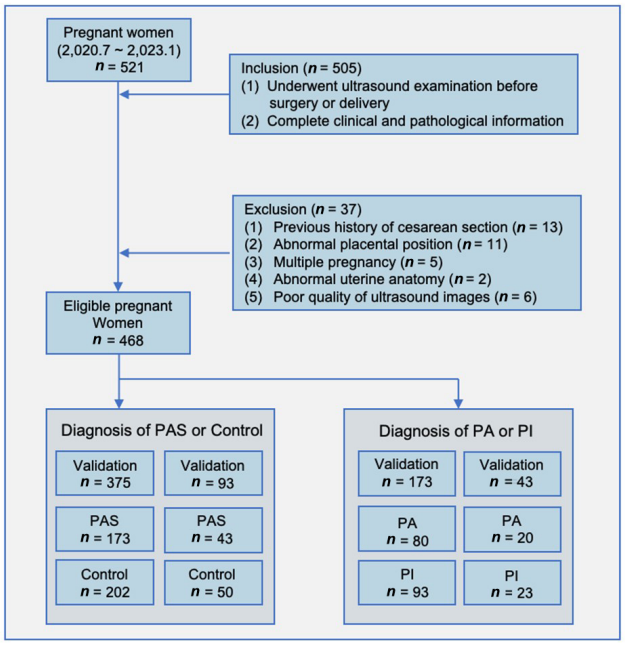

Figure 1. Flowchart for screening pregnant women participating in this study, including the control, PAS, PA and PI groups. PA, placenta accreta; PAS, placenta accreta spectrum; PI, placenta increta.

Acquisition and pre-processing of ultrasound images

All pregnant women were tested using a color Doppler ultrasound diagnostic instrument (Samsung HERA W10, USA) with a CA 2–9A convex array probe. The frequency was set to 2.0-9.0 MHz. Each pregnant woman assumed a supine position, with the bladder appropriately filled and the lower abdomen fully exposed. Images with the largest area of connection between the placenta and the uterus were displayed on the same screen, captured, and saved in the Joint Photographic Experts Group format. All images were collected within one week before the termination of pregnancy.

Establish EA-EffV2Net with edge attention module and momentum-contrast pre-trained weight

EfficientV2 was employed as the backbone network, which was constructed by stacking mobile inverted bottleneck convolutional neural network (MBConv) blocks and Fused-MBConv.[17] Currently, the clinical diagnosis of PA and PI is based on the depth of invasion of trophoblast cells into the uterine wall. Thus, capturing sufficient information from the placental margin and uterine wall was crucial for our task. This study proposed an edge attention mechanism (EAM) module to focus on the edge information in ultrasound images. The EAM was designed to possess the capability to model edge maps in each feature channel with limited resources. Weights were assigned according to the

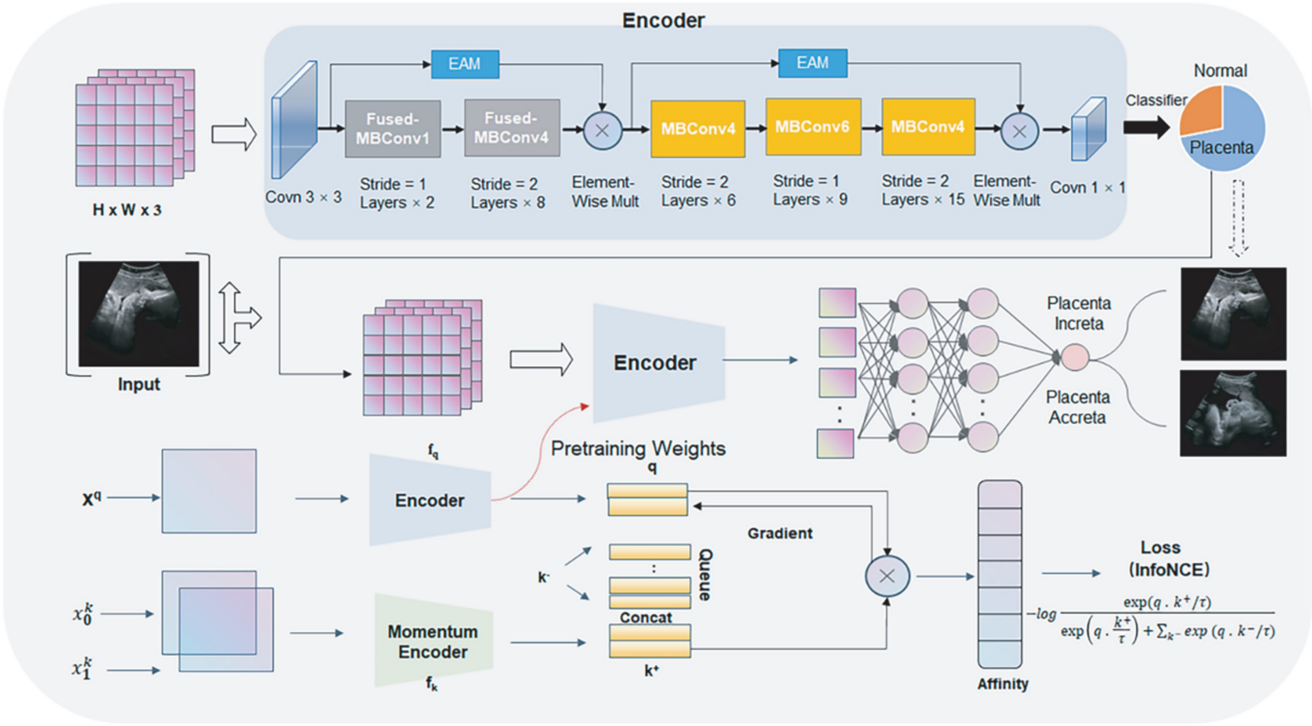

Figure 2. Flowchart depicting the EA-EffV2Net model used in this study.

importance of different feature channels, and spatially separable convolutions (SSCs) were employed to process the spatial dimensions of images and convolution kernels from width and height. An EAM module was constructed and fused the last layer of the features map extracted from both the Fused-MBconv and MBConv blocks in the original EfficientV2 network *via* skipping connections; this was to enhance edge information in low-level and high-level semantic features, respectively, thereby allowing EA-EffV2Net to capture more edge positional features.

To alleviate the problem of insufficient training data because of the limited sample size, a self-supervised momentum contrast (MoCo) model was introduced to improve the network's learning capability by assigning the pre-trained weight of the encoding phase to EA-EffV2Net. The MoCo comprised an encoder, a momentum encoder, and a queue. The pre-trained weight of the encoder of EA-EffV2Net was obtained by training the self-supervised MoCo model.[18] Figure 2 presents the flowchart of the proposed EA-EffV2Net model.

Training and validating the models

A total of 1573 ultrasound images were obtained from the 468 pregnant women enrolled and were used for training and evaluating the CNNs. All image data were divided randomly at an 8∶2 ratio into a training set containing 1260 images (688 PAS, 304 PA, and 268 PI) and a validation set containing 313 images (172 PAS, 75 PA, and 66 PI). The size of the input image was adjusted uniformly to 224 × 224 pixels before the images were fed to the models. The EA-EffV2Net was trained for 100 epochs using a learning rate of 0.0125 and a batch size of 32. The self-supervised MoCo model was trained for 200 epochs using a batch size of 256 and a learning rate of 0.0300. The stochastic gradient descent optimizer was utilized with EA-EffV2Net and MoCo, with a weight decay rate of 0.0001 and a momentum update value of 0.9000. The ImageNet-1K dataset used in the comparison experiments is available for download from https://image-net.org.

The receiver operating characteristic (ROC), area under the receiver operating characteristic curve (AUC), accuracy, precision, recall, and F1 score were employed to assess the results obtained from the models. Confusion matrices were drawn to show in detail the scoring ability of the EA-EffV2Net model. The gradient-weighted class activation mapping (Grad-CAM) technique was used to visualize the diagnostic results. All experiments were conducted on a workstation with an NVIDIA GeForce RTX 3090 Ti GPU, an Intel Core i9-12900 CPU (2.4 GHz), and 32 GB of RAM.

Statistical analysis and development of the clinical model

The *Kruskal-Wallis* test was used for non-normally distributed data and a *Chi-squared* test was used to

Table 1: Statistical results of patients' clinical characteristics

	Control (*n* = 252)	PA (*n* = 100)	PI (*n* = 116)	*P*-value
Age (years)	30.46 ± 3.43	31.63 ± 4.31	31.17 ± 4.99	0.036
GA at delivery (weeks)				<0.01
⩽34	0	6 (6.0)	7 (6.0)	
>34 to 40	174 (69.1)	70 (70.0)	80 (69.0)	
>40–41	58 (23.0)	18 (18.0)	22 (19.0)	
> 41	20 (7.9)	6 (6.0)	7 (6.0)	
BMI	28.15 ± 3.79	28.60 ± 3.39	28.80 ± 3.48	0.234
Prenatal HGB (g/L)	120.19 ± 11.09	121.09 ± 11.83	119.6 ± 10.91	0.652
Postpartum HGB (g/L)	112.65 ± 14.99	108.45 ± 14.00	97.66 ± 15.55	<0.01
Abortion times				<0.01
0	175 (69.4)	41 (41.0)	54 (46.6)	
1	49 (19.4)	40 (40.0)	36 (31.0)	
2	23 (9.1)	13 (13.0)	14 (12.1)	
⩾3	5 (2.0)	6 (6.0)	12 (10.3)	
Previous deliveries times				<0.01
0	198 (78.6)	73 (73.0)	90 (77.6)	
1	49 (19.4)	26 (26.0)	24 (20.7)	
⩾2	5 (2.0)	1 (1.0)	2 (1.7)	
ART				<0.01
Yes	2 (0.8)	1 (1.0)	6 (2.4)	
No	250 (99.2)	99 (99.0)	110 (94.8)	
Progesterone				<0.01
Yes	11 (4.4)	13 (13.0)	27 (23.3)	
No	241 (95.6)	87 (87.0)	89 (8.1)	
Prenatal vaginal bleeding				<0.01
Yes	4 (1.6)	14 (14.0)	20 (17.2)	
No	248 (98.4)	86 (86.0)	96 (82.8)	
Estimated blood loss (ml)				<0.01
<1000	249 (98.8)	96 (96.0)	67 (57.8)	
⩾1000	3 (1.2)	4 (4.0)	49 (41.2)	
Anterior placenta				0.042
Yes	136 (54.0)	66 (66.0)	54 (4.9)	
No	116 (46.0)	34 (34.0)	62 (53.4)	

Data are presented as mean ± SD for normally distributed continuous variables, median (interquartile range) for non-normally distributed continuous variables (including gestational age at delivery, abortion times, previous delivery times, ART, progesterone, prenatal vaginal bleeding, estimated blood loss, and anterior placenta), and *n* (%) for categorical variables. PA, placenta accreta; PI, placenta increta; GA, gestational age; BMI, body mass index; HGB, hemoglobin; ART, assisted reproductive technology. The Kruskal-Wallis test was used for non-normally distributed data, and a Chi-squared test was used to evaluate differences in the categorical clinical factors.

evaluate differences in the categorical clinical factors in this study.[19,20] Clinical factors with $P < 0.05$ were considered statistically significant and were used to build the clinical model. Subsequently, significant clinical factors were included, and clinical models were developed using logistic regression analysis.[21]

RESULTS

Clinical characteristics

Based on the inclusion and exclusion criteria, we finally enrolled 468 pregnant women in our study, of which 252 had a normal placenta and 216 had histologically confirmed PA or PI, respectively. The maternal age, gestational age at delivery, postpartum hemoglobin, abortion times, previous delivery times, assisted reproductive technology (ART) application, progesterone use, prenatal vaginal bleeding, estimated blood loss, and placenta position were significantly different ($P < 0.05$) among the control, PA and PI groups (Table 1). These factors were then used to develop the clinical model for the detection of PAS and the differential diagnosis of PA and PI. Neither body mass index nor prenatal hemoglobin showed a significant difference based on the statistical analysis results ($P > 0.05$, Table 1).

Table 2: Performance comparisons of EA-EffV2Net *vs.* different strategies

	Task	AUC	Accuracy	Precision	Recall	F1 score
EfficientnetV2	PAS *vs.* Control	0.8934	0.8981	0.9018	0.8935	0.8962
	PA *vs.* PI	0.7323	0.7324	0.7318	0.7323	0.7319
EfficientnetV2 + EAM	PAS *vs.* Control	0.9257	0.9268	0.9263	0.9258	0.9260
	PA *vs.* PI	0.7782	0.7817	0.7841	0.7782	0.7792
EfficientnetV2 + MoCo pre-trained weight	PAS *vs.* Control	0.9320	0.9348	0.9302	0.9321	0.9311
	PA *vs.* PI	0.7840	0.7887	0.7946	0.7841	0.7853
EfficientnetV2 + EAM + MoCo pre-trained weight	PAS *vs.* Control	0.9369	0.9363	0.9351	0.9369	0.9359
	PA *vs.* PI	0.7998	0.8028	0.8049	0.7998	0.8009

AUC, area under the receiver operating characteristic curve; EAM: edge attention mechanism; MoCo, momentum contrast; PAS, placenta accreta spectrum; PA, placenta accreta; PI, placenta increta.

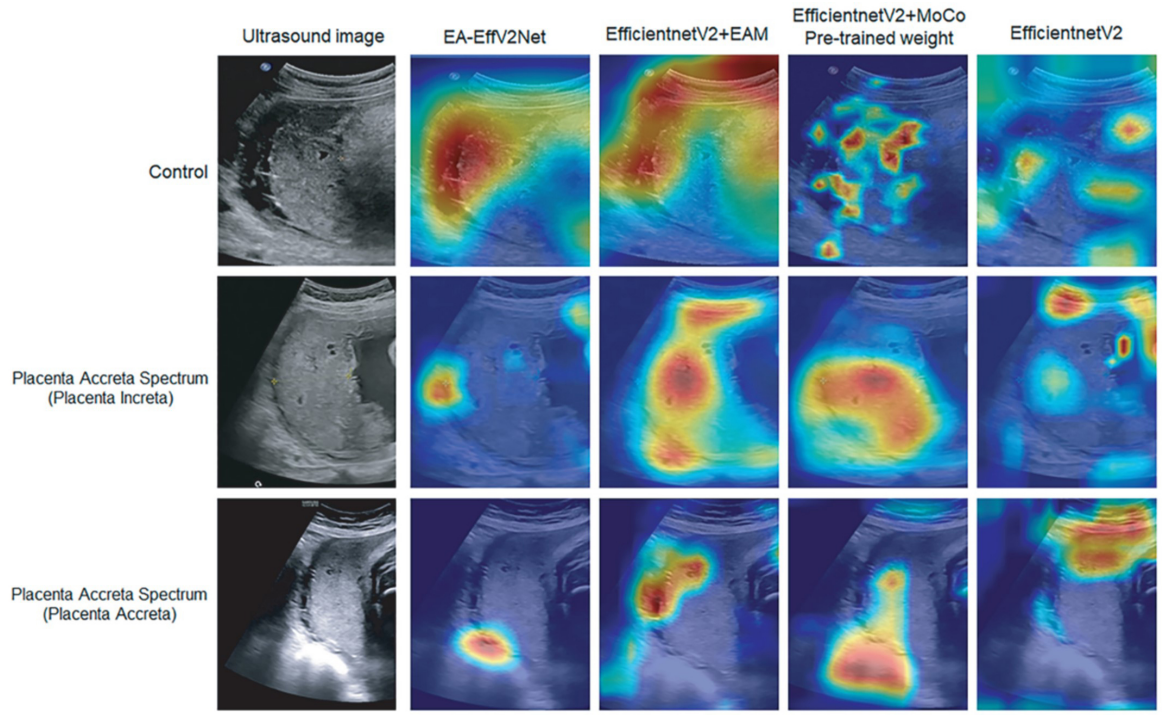

Figure 3. Visualizations of the models in ultrasound images by Grad-CAM. The first row shows heatmaps of the ultrasound images without PAS. The second and third rows show heatmaps of the ultrasound images with PA and PI, respectively. Ultrasound images are obtained transabdominally by color Doppler ultrasound diagnostic instrument (Samsung HERA W10, USA) with a CA 2-9A convex array probe. The frequency was set to 2.0-9.0 MHz. Each pregnant woman assumed a supine position, with the bladder appropriately filled and the lower abdomen fully exposed. Images with the largest area of connection between the placenta and the uterus were displayed on the same screen, captured, and saved in the Joint Photographic Experts Group format. Grad-CAM, gradient-weighted class activation mapping; PA, placenta accreta; PAS, placenta accreta spectrum; PI, placenta increta.

Comparison of EA-EffV2Net model with different strategies

As shown in Table 2, EfficientnetV2 with a MoCo pre-trained weight yielded a slightly improved AUC compared with that of EfficientnetV2 with EAM. By adding both the EAM and the MoCo pre-trained weight to EfficientnetV2, EA-EffV2Net generated much higher AUC, accuracy, precision, recall, and F1 scores compared with EfficientnetV2 for the detection of PAS and the differential diagnosis of PI and PA.

Heatmaps (Figure 3) were generated on ultrasound images by gradient-weighted class activation mapping for a better understanding of the features learned by EfficientnetV2, EfficientnetV2 + MoCo pre-trained weight, EfficientnetV2 + EAM, and our EA-EffV2Net. The results were consistent with our clinical experience. Furthermore, the results showed that the integration of attention modules improved the network's capability to focus on the edge of the placenta. For the detection of PAS, the models with attention modules (EfficientnetV2 + EAM and EfficientnetV2 + EAM + MoCo pre-trained weight) tended to focus on a wide range of edges, while for the differential diagnosis of PA and PI,

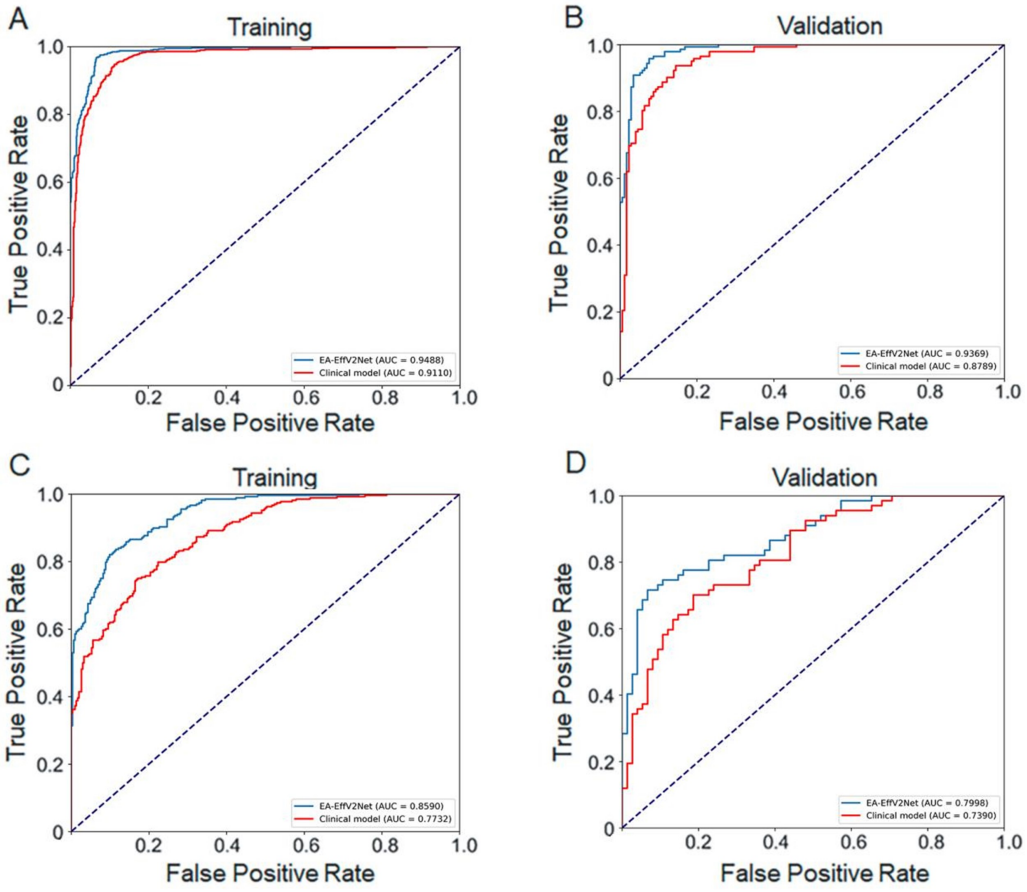

Figure 4. Receiver operating characteristic curves of EA-EffV2Net and the clinical model for diagnosing PAS in the (A) training and (B) validation sets and for the differential diagnosis of PI and PA in the (C) training and (D) validation sets. PA, placenta accreta; PAS, placenta accreta spectrum; PI, placenta increta.

the models with attention modules focused on a refined range of edges.

Comparison of EA-EffV2Net model and the clinical model

The diagnostic performance of EA-EffV2Net and the developed clinical model are compared and listed in Table 3. Generally, EA-EffV2Net yielded a higher AUC compared with the clinical model for the detection of PAS and the differential diagnosis of PI and PA. Figure 4 depicts the ROC curves of EA-EffV2Net and the clinical model on training and validation sets. Confusion matrices of EA-EffV2Net and the clinical model are presented in Figure 5. Compared with the clinical diagnostic model, EA-EffV2Net generated slightly higher misdiagnosis rates when diagnosing PAS and PA. However, the clinical model generated higher missed diagnosis rates when diagnosing PAS and PI.

DISCUSSION

Main findings

This study applies the EAM module and self supervised MoCo pre-training weights to improve the diagnostic ability of ultrasound for placental invasion. The results indicate that both clinical models and ultrasound based EA-EffV2Net models can diagnose placental invasion, but this effect is better performed on EA-EffV2Net. The study reports the first attempt at developing a deep learning method for the ultrasound-based diagnosis of placental invasion in pregnant women. It can provide the probability of PAS events and increase clinical sensitivity; at the same time, as its forward-looking judgment, it provides an opportunity to systematically evaluate the occurrence of PA or PI before termination of pregnancy, and ultimately reduce the incidence of adverse events of pregnancy.

Results in the context of what is known

We analyzed various clinicopathological factors that may be correlated to the status of placental invasion. According to previous reports, a history of cesarean section and placenta previa are the two strongest risk factors for PAS.[22] Additionally, multiple pregnancies[23] and uterine anomalies[24] are considered high risk factors in some cases. When pregnant women possess PAS-

Table 3: Performances of EA-EffV2Net and the clinical model on training and validation sets

Model	Task	Dataset	AUC	Accuracy	Precision	Recall	F1 score
Clinical model	PAS *vs.* Control	Training	0.9110	0.9095	0.9082	0.9110	0.9090
		Validation	0.8789	0.8822	0.8830	0.8789	0.8805
	PA *vs.* PI	Training	0.7732	0.7780	0.7818	0.7732	0.7745
		Validation	0.7390	0.7394	0.7387	0.7390	0.7388
EA-EffV2Net	PAS *vs.* Control	Training	0.9488	0.9468	0.9456	0.9488	0.9465
		Validation	0.9369	0.9363	0.9351	0.9369	0.9359
	PA *vs.* PI	Training	0.8590	0.8619	0.8644	0.8590	0.8605
		Validation	0.7998	0.8028	0.8049	0.7998	0.8009

AUC, area under the receiver operating characteristic curve; PAS, placenta accreta spectrum; PA, placenta accreta; PI, placenta increta.

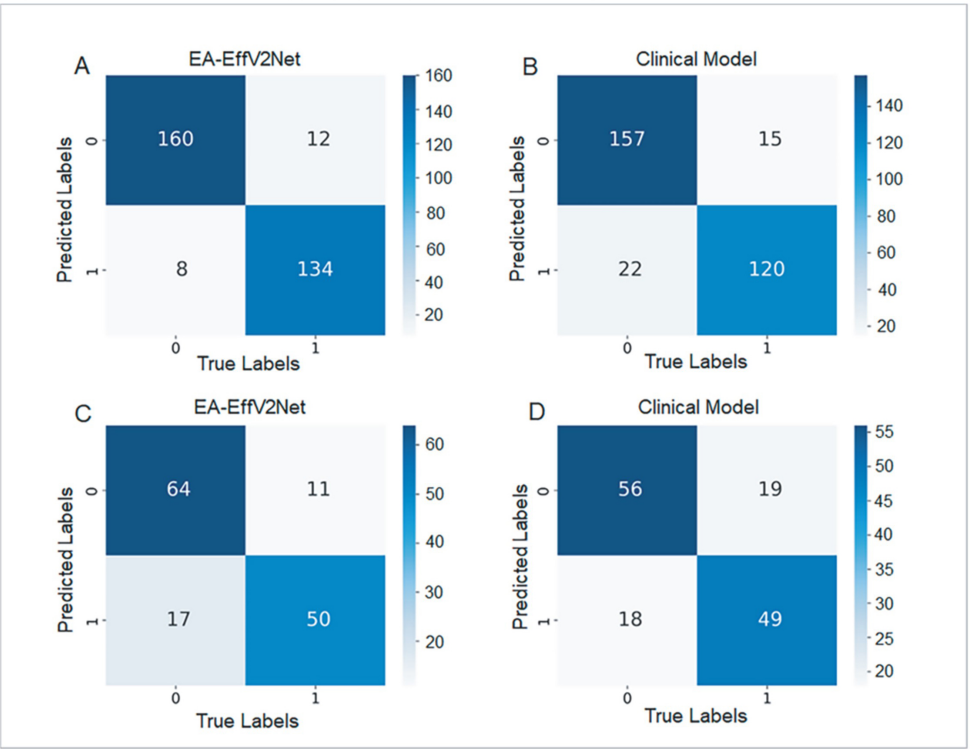

Figure 5. Confusion matrices of EA-EffV2Net (A and C) and the clinical model (B and D) for diagnosing PAS (A and B) and differentially diagnosing PA and PI (C and D). PA, placenta accreta; PAS, placenta accreta spectrum; PI, placenta increta.

related risk factors, especially high-risk ones, obstetricians will make sufficient preparations before terminating a pregnancy to avoid potential adverse outcomes. However, in clinical practice, many pregnant women do not have a history of cesarean section or placenta previa, which makes it hard for clinicians to perform the timely determination of placental invasion. In such cases, the ultrasound signs of PAS are not prominent and can lead to inadequate preparation before surgery or delivery, thereby increasing the incidence of postpartum hemorrhage, postpartum infection, and even hysterectomy. Therefore, unlike previous reports,[25,26] this study excluded cases with strong risk factors (such as history of cesarean section or abnormal placental position) to realize the diagnosis of PAS in a low-risk population. We finally identified 10 clinical factors to be strongly associated with the status of placental invasion (Table 1, $P < 0.05$), among which, maternal age, estimated blood loss,[25,26] a history of miscarriage,[27] and ART [28] were previously reported to be related to PAS. The developed clinical models based on the identified 10 factors showed good performance for diagnosing PAS and differentially diagnosing PA and PI.

Clinical implications

Previous studies have indicated that textural features derived from the magnetic resonance imaging (MRI) images of pregnant women can be used to reflect the

status of placental invasion.[29,30] Previously published works focused on MRI data and used machine learning methods, which involve tedious steps. However, clinical MRI screening is not suitable for all patients due to hypersensitivity to the MRI contrast agent and high examination fees, especially for low-risk pregnant women.[31] Our model is built on the basis of routine ultrasound examination, without additional examination costs for pregnant women. At the same time, the operation is simple, and there will be no adverse reactions such as allergies that may be caused by MRI.

Strengths and limitations

It is necessary to improve the diagnostic ability of PAS through non-invasive examination methods such as ultrasound before terminating pregnancy. However, our model still has some limitations: currently, the data for the establishment of the model comes from one regional medical center in China, and the sample size is relatively limited. We will further expand the scale and scope of verification on the current basis and conduct verification in more regional medical centers.

Conclusion and implications

This study proposed a novel EA-EffV2Net model for the diagnosis of PAS and the differential diagnosis of PA and PI based on ultrasound images. This model can improve the diagnostic efficiency of ultrasound for PAS, which increase the safety of clinical work, and reduce the incidence of adverse pregnancy outcomes.

DECLARATION

Acknowledgement

The authors have no acknowledgements to declare.

Author contributions

Shi B and Jiang XR: Conceptualization, Methodology, Project administration; Gao WY, You SL, and Wu YJ: Data curation, Investigation, Writing – original draft; Gao WY, You SL, Wu YJ: Formal analysis; Gao WY, You SL, Wu YJ, Su J, and Li ZW: Writing – review and editing. All authors have accepted responsibility for the entire content of this submitted manuscript and approved submission.

Source of funding

None.

Ethical approval

The study was approved by the ethics committee of the First Affiliated Hospital of China Medical University (No. 2024241).

Informed consent

Participating women provided signed informed consent.

Conflict of interest

The authors confirm that there are no conflicts of interest.

Use of large language models, AI and machine learning tools

No artificial intelligence (AI) tools or large language models (LLMs) were used in the design, conduct, analysis, or writing of this study.

Data availability statement

Not applicable.

REFERENCES

1. Luke RK, Sharpe JW, Greene RR. Placenta accreta: the adherent or invasive placenta. *Am J Obstet Gynecol.* 1966;95(5):660–668.
2. Bartels HC, Postle JD, Downey P, Brennan DJ. Placenta accreta spectrum: a review of pathology, molecular biology, and biomarkers. *Dis Markers.* 2018;2018:1507674.
3. Klar M, Michels KB. Cesarean section and placental disorders in subsequent pregnancies—a meta-analysis. *J Perinat Med.* 2014;42(5):571–583.
4. Creanga AA, Bateman BT, Butwick AJ, et al. Morbidity associated with cesarean delivery in the United States: is placenta accreta an increasingly important contributor? *Am J Obstet Gynecol.* 2015;213(3):384.e381–311.
5. Cheng KK, Lee MM. Rising incidence of morbidly adherent placenta and its association with previous caesarean section: a 15-year analysis in a tertiary hospital in Hong Kong. *Hong Kong Med J.* 2015;21(6):511–517.
6. Sentilhes L, Merlot B, Madar H, Sztark F, Brun S, Deneux-Tharaux C. Postpartum haemorrhage: prevention and treatment. *Expert Rev Hematol.* 2016;9(11):1043–1061.
7. Silver RM. Abnormal placentation: placenta previa, Vasa previa, and placenta accreta. *Obstet Gynecol.* 2015;126(3):654–668.
8. Solheim KN, Esakoff TF, Little SE, Cheng YW, Sparks TN, Caughey AB. The effect of cesarean delivery rates on the future incidence of placenta previa, placenta accreta, and maternal mortality. *J Matern Fetal Neonatal Med.* 2011;24(11):1341–1346.
9. Garmi G, Salim R. Epidemiology, etiology, diagnosis, and management of placenta accreta. *Obstet Gynecol Int.* 2012;2012:873929.
10. Jauniaux E, Collins SL, Jurkovic D, Burton GJ. Accreta placentation: a systematic review of prenatal ultrasound imaging and grading of villous invasiveness. *Am J Obstet Gynecol.* 2016;215(6):712–721.
11. Jauniaux E, Bhide A. Prenatal ultrasound diagnosis and outcome of placenta previa accreta after cesarean delivery: a systematic review and meta-analysis. *Am J Obstet Gynecol.* 2017;217(1):27–36.
12. Jauniaux E, Collins S, Burton GJ. Placenta accreta spectrum: pathophysiology and evidence-based anatomy for prenatal ultrasound imaging. *Am J Obstet Gynecol.* 2018;218(1):75–87.
13. Baughman WC, Corteville JE, Shah RR. Placenta accreta: spectrum of US and MR imaging findings. *Radiographics.* 2008;28(7):1905–1916.
14. Collins SL, Ashcroft A, Braun T,*et al.* Proposal for standardized ultrasound descriptors of abnormally invasive placenta (AIP). *Ultrasound Obstet Gynecol.* 2016;47(3):271–275.
15. Zhou SK, Greenspan H, Davatzikos C, *et al.* A review of deep learning in medical imaging: Imaging traits, technology trends, case studies with progress highlights, and future promises. *Proc IEEE Inst Electr Electron Eng.* 2021;109(5):820–838.
16. Li H, Bhatt M, Qu Z, Zhang S, Hartel MC, Khademhosseini A, *et al.* Deep learning in ultrasound elastography imaging: a review. *Med Phys.* 2022;49(9):5993–6018.

17. Tan M,X Le QV. EfficientNetV2: Smaller Models and Faster Training. Paper presented at the Proceedings of the 38th International Conference on Machine Learning, *Proceedings of Machine Learning Research*, 2021;139:10096-10106. https://proceedings.mlr.press/v139/tan21a.html
18. He K, Fan H, Wu Y, Xie S, Girshick R. Momentum contrast for unsupervised visual representation learning. *2020 IEEE/CVF Conference on Computer Vision and Pattern Recognition (CVPR)*. June 13-19, 2020. Seattle, WA, USA. IEEE, 2020: 9726-9735.
19. Fan C, Zhang D, Zhang CH. On sample size of the kruskal-Wallis test with application to a mouse peritoneal cavity study. *Biometrics*. 2011;67(1):213–224.
20. Roman H. Statistics in medicine: Mann and Whitney test. *Gynecol Obstet Fertil*. 2009;37(2):208–209.
21. Tibshirani R. Regression shrinkage and selection *via* the lasso: a retrospective. *J R Stat Soc Ser B Stat Methodol*. 2011;73(3):273–282.
22. Berkley EM, Abuhamad A. Imaging of placenta accreta spectrum. *Clin Obstet Gynecol*. 2018;61(4):755–765.
23. DI Girolamo R, Buca D, Galliani C, *et al*. Systematic review and meta-analysis on placenta accreta spectrum disorders in twin pregnancies: risk factors, detection rate and histopathology. *Minerva Obstet Gynecol*. 2023;75(1):55–61.
24. Henriet E, Roman H, Zanati J, Lebreton B, Sabourin J-C, Loic M. Pregnant noncommunicating rudimentary uterine horn with placenta percreta. *JSLS*. 2008;12(1):101–103.
25. Shao Q, Xuan R, Wang Y, *et al*. Deep learning and radiomics analysis for prediction of placenta invasion based on T2WI. *Math Biosci Eng*. 2021;18(5):6198–6215.
26. Hu Y, Chen W, Kong C, *et al*. Prediction of placenta accreta spectrum with nomogram combining radiomic and clinical factors: a novel developed and validated integrative model. *Int J Gynaecol Obstet*. 2023;162(2):639–650.
27. Kyozuka H, Yamaguchi A, Suzuki D, *et a*l. Risk factors for placenta accreta spectrum: findings from the Japan environment and Children's study. *BMC Pregnancy Childbirth*. 2019;19(1):447.
28. Baldwin HJ, Patterson JA, Nippita TA, *et al*. Antecedents of abnormally invasive placenta in primiparous women: risk associated with gynecologic procedures. *Obstet Gynecol*. 2018;131(2):227–233.
29. Sun H, Qu H, Chen L,, *et al*. Identification of suspicious invasive placentation based on clinical MRI data using textural features and automated machine learning. *Eur Radiol*. 2019;29(11):6152–6162.
30. Xuan R, Li T, Wang Y, Xu J, Jin W. Prenatal prediction and typing of placental invasion using MRI deep and radiomic features. *Biomed Eng Online*. 2021;20(1):56.
31. Mittendorff L, Young A, Sim J. A narrative review of current and emerging MRI safety issues: What every MRI technologist (radiographer) needs to know. *J Med Radiat Sci*. 2022;69(2):250–260.